Self-templating growth of copper nanopearl-chain arrays in electrodeposition

Yu-Yan Weng, Bo Zhang, Shao-Jie Fu, Mu Wang,* Ru-Wen Peng, Guo-Bin Ma, Da-Jun Shu, and Nai-Ben Ming
National Laboratory of Solid State Microstructures and Department of Physics, Nanjing University, Nanjing 210093, China
(Received 1 January 2010; published 25 May 2010)

We report here a unique in-plane self-templating electrochemical growth of arrays of copper nanopearl chains from an ultrathin layer of $CuSO_4$ electrolyte. Scanning electron microscopy indicates that the electrodeposit filaments form equally spaced bundles, which consist of long, straight, pearl-chain-like copper filaments with corrugated periodic structure. The bundle separation can be tuned by changing the applied electric current in electrodeposition. Experiments show that the periodic morphology on the nanopearl chain corresponds to the periodic distribution of copper and cuprous oxide. The mechanism for the bundle formation is discussed.

DOI: 10.1103/PhysRevE.81.051607 PACS number(s): 68.70.+w, 62.23.St, 81.07.−b, 81.15.Pq

I. INTRODUCTION

Microstructured metallic filament arrays have attracted much attention in recent decades due to their fascinating physicochemical properties and unique applications [1–4]. Electrochemical deposition is an easy and effective way to fabricate metallic structures, and nowadays large-scale implementation of chemical solution processing approaches has been greatly facilitated by commercial availability of templates, such as anodic aluminum oxide (AAO) or polymeric membranes. Yet the destructivity during removal of the template becomes a nonignorable drawback for many applications [2]. Is there any way to create robust metallic structures on a substrate by electrochemical deposition? Thus far, two approaches have been invented by Fleury *et al.* [5–9] and Wang *et al.* [10,11] independently, which allow to electrochemically deposit metallic structures robustly on a substrate. According to the method proposed by Fleury *et al.* [5], gold clusters are initially sputtered on the substrate surface, with cluster concentration lower than the critical value for electric percolation. With such precoated gold clusters, copper deposits can easily develop horizontally over the substrate surface and the deposit branches are rough and fractal-like [5]. For the method of Wang *et al.* [10,11], an ultrathin electrolyte layer just a few hundreds of nanometers in thickness is created above the substrate surface, in which metallic filaments with spontaneous periodic corrugations are electrodeposited. With this method, the tip-splitting rate has been decreased significantly comparing to that grown with other methods and the deposit branches become much smoother. Even so, exact control of spatial distribution of tip-splitting remains challenging. Very recently, Zhang *et al.* [12] reported a new approach using corner-mediated electrodeposition to fabricate regular metallic filament arrays. Although in-plane template is used, the width of metallic filaments is independent of the template size. Instead, the filament width is controlled by the applied electric voltage or current in electrodeposition [12]. Despite of the excellent controllability in fabricating in-plan metallic filament arrays with this method, real application of these metallic filaments still awaits a breakthrough in introducing periodic corrugations on these filaments, which are essential to couple electromagnetic waves to metal surface and to excite the surface plasmon polariton [13–17].

Surface plasmon polariton is a charge density wave on metal surface. The dispersion relation of the surface plasmon polariton is exponentially related to the wave vector, in contrast to the linear relation of the free transmission light wave in space [13]. By introducing periodic structures on the metal surface, the surface plasmon polariton gets back-folded and this back-folded mode crosses the light dispersion line. Therefore, microstructured metallic filaments can play the role of waveguide especially in the infrared and THz region [16,17]. Conventionally, photolithography process is applied to fabricate these microstructures. Despite of accuracy and controllability of photolithography, the cost and time of fabrication are the important factors that one has to consider.

The spontaneous oscillations observed in ultrathin electrodeposition system [10,11,17] can be applied to generate metallic microstructures bottom-up for plasmonics studies. For example, with the ultrathin electrolyte layer, we have fabricated single-crystalline silver filaments with periodic pearl-chain-like structure on silicon wafer [17]. Fourier transform infrared spectroscopy, infrared focus-plane-array imaging, and numerical simulations demonstrate that the excited surface waves may sustain on the silver "pearl chains" in midinfrared range. Based on propagation features of the surface waves on silver filaments, we suggested that such a structure might be applied as a waveguide in mid-infrared range [17].

The spatial periodicity of the corrugation is important in coupling the electromagnetic wave to the metallic filaments and it strongly depends on the applied electric voltage or current [11]. In our previous experiments, the applied voltage or current was increased so as to achieve shorter spatial periodicity on the filaments. During the experiments, we observed that very often, the filaments mysteriously formed parallel bundles and the separation of the neighboring bundles depended on experimental conditions. In this paper, we focus on the physical origin of the bundle formation mechanism. Scanning electron microscopy indicates that equally spaced bundles consist of long, straight pearl-chain-like copper filaments. This growth behavior occurs only when the electrodeposition rate becomes high. Based on experimental observations, we conclude that the bundle forma-

*Author to whom correspondence should be addressed; muwang@nju.edu.cn

tion is a self-templating process and is due to the instability of melting interface of electrolyte ice in ultrathin layer electrodeposition.

II. EXPERIMENTAL

The electrodeposition was carried out in a cell consisting of two parallel, straight electrodes made of copper wires 0.5 mm in diameter (99.99% pure, Goodfellow). The separation of electrodes was fixed as 1.0 cm. The electrodes were bounded by two rigid boundaries (conventional microscope slice and polished silicon wafer, respectively). The electrolyte solution was prepared by dissolving analytical regent $CuSO_4$ in deionized, ultrapure water (Millipore, electric resistivity 18.2 $M\Omega$ cm). The initial concentration of $CuSO_4$ aqueous electrolyte was 0.05 M. In order to generate the ultrathin electrolyte layer for electrodeposition, a programmable constant temperature circulator (Polystat 12108-35, Cole Parmer) and a Peltier element were used to nucleate the ice of electrolyte and to solidify electrolyte. Detailed description of experimental system has been reported in Refs. [10,11]. The flux of dried nitrogen gas flowed through the sealed chamber to prevent water condensation on glass window of the deposition cell, so the processes of electrolyte solidification and electrodeposition could be monitored *in situ* with optical microscopy. The temperature of electrodeposition cell was decreased to −4 °C gradually. During the solidification of electrolyte, $CuSO_4$ was partially expelled from the ice of electrolyte due to the segregation effect, which increased the local concentration of $CuSO_4$ in front of the solid-liquid interface [10–12]. Hence, local solidification temperature was further decreased. This process continued until equilibrium was reached. Meanwhile, an ultrathin layer of concentrated $CuSO_4$ electrolyte was trapped between the ice of electrolyte and the glass plates of the electrodeposition cell, in which the electrodeposition experiment was carried out. The thickness of this ultrathin layer depended on temperature, initial concentration of electrolyte, and the amount of electrolyte solution in the deposition cell [11]. In our system, the typical thickness of this layer was of the order of several hundreds of nanometers.

In order to avoid grain boundaries of ice in solidifying the electrolyte, which might introduce additional structures to the electrodeposit morphology [11], repeated solidification and melting were applied with the help of a Peltier element underneath the electrodeposition cell, until only one or just a few nuclei of ice remained in the deposition cell. The temperature decreasing rate was kept as low as about 0.1 °C/h in order to resume a flat solid-liquid interface in solidifying the electrolyte.

Electrodeposition was carried out in galvanostatic mode. A constant current power supplier provided the output current in the range of 15–50 μA. When the constant current was applied, copper filaments initiated from the cathode, deposited robustly on the substrate surface, and developed toward the anode.

When electrodeposition was finished, the electrodeposits were thoroughly rinsed with deionized water and dried in nitrogen atmosphere. A field-emission scanning electron microscope (LEO 1530VP) was used to observe the deposit morphology and to analyze the chemical components along the deposit filament. The concentration profile in front of the growing interface was observed with optical interference contrast microscopy (Leitz Orthro-Plan Pol).

III. RESULTS AND DISCUSSIONS

In our experimental system, we find that when the applied electric current is below 15 μA and the copper filaments deposit firmly on the substrate surface and are fractal-like, as that reported in Refs. [10–12]. When the applied electric current exceeds 15 μA, however, the deposit morphology changes dramatically to an equally spaced bundle pattern, as shown in Fig. 1(a). Scanning electron microscopy indicates that each bundle consists of long, straight, periodically nanostructured "pearl chains" [Fig. 1(b)]. The detailed feature of the pearl chains is illustrated in Fig. 1(c), where each copper "pearl" is about a few hundreds of nanometers in size.

In galvanostatic electrodeposition, spontaneous oscillation of electric voltage has been measured across the electrodes, as shown in Fig. 1(d). Fourier transform of the measured voltage signal indicates that the oscillation is indeed periodic, as illustrated in the inset of Fig. 1(d).

Our previous studies indicate that such a spontaneous oscillation is associated with the alternating electrodeposition of copper and cuprous oxide in the ultrathin electrodeposition system, with cuprous oxide dominates in the junction regions between neighboring beads [11]. In fact, alternating (planar) electrodeposition of the Cu and Cu_2O has already been reported before when a forced oscillating electric signal was applied [18]. To identify the situation in this system, we analyze the chemical components with energy dispersive x-ray analysis (EDS) along the marked lines in Fig. 2(a), where the copper filaments were deposited on the surface of silicon wafer. Figure 2(b) shows the analysis along the solid red line, which goes through the central part of the filament. The upper one shows that the distribution of oxygen along the line and the lower one shows the distribution of copper along the line. It is clear that oxygen is more concentrated in the junction regions of the pearl chain. Figure 2(c) shows the EDS analysis along the dashed white line, which cuts across the edge of the filament, and some segments just locate on the silicon substrate. The upper graph shows the oxygen profile and the lower graph illustrates the distribution of copper. It is clear that the oxygen concentration is much lower on the surface of silicon substrate than that on the filament. This means that the richer concentration of oxygen at the junction region of the pearl chain is indeed the intrinsic feature of the filament and excludes the possible contribution of oxidation layer on the silicon surface.

Due to the geometrical confinement of the ultrathin electrolyte layer, the electric resistance between two electrodes is usually high in electrodeposition. When a constant current is applied across the electrodes, the joule heat is generated in front of the growing tips of the electrodeposits. When the electric current is increased sufficiently high, the generated heat in electrodeposition cannot be released in time, which may locally melt the ice in front of the growing tips and

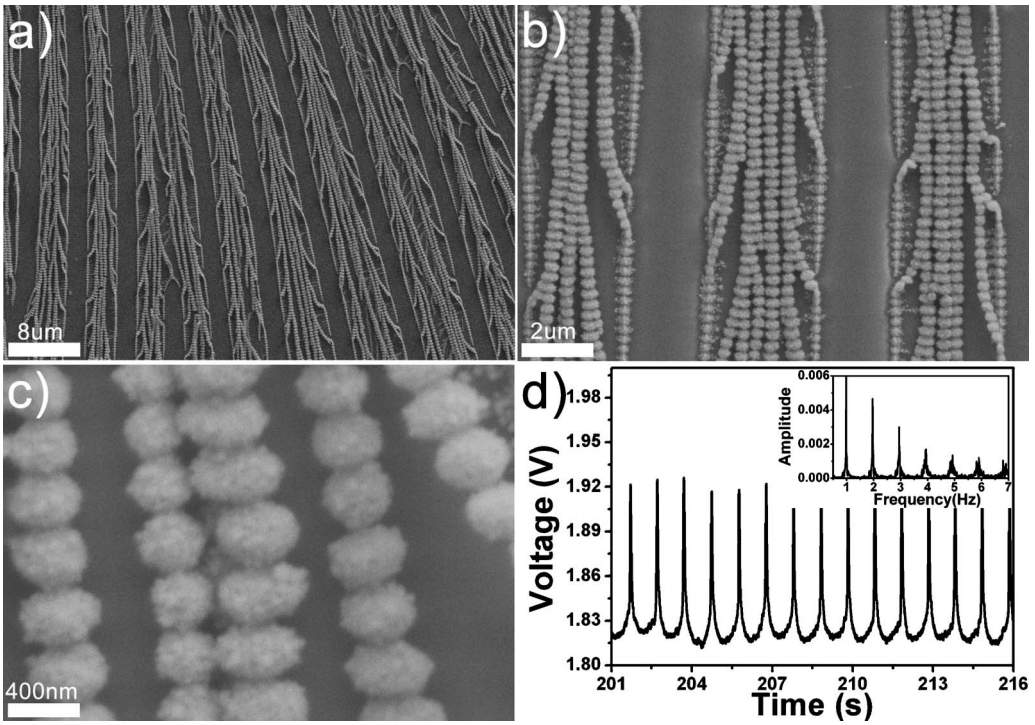

FIG. 1. (a) Scanning electron micrograph of the bundles of copper filaments electrodeposited at 30 μA. (b) The bundles observed with higher magnification. Some filaments are bent to the edge of the bundle, suggesting the existence of a crust (ice wall of the melted channel) along the bundle in electrodeposition. Periodic corrugations can be identified on the filaments. (c) Further enlarged micrograph to show that each bundle consists of beads of copper crystallites. (d) The oscillating voltage signal measured across the electrodes in galvanostatic electrodeposition. (Inset) Fourier transform indicates that the oscillation is indeed periodic.

hence embed channels of aqueous electrolyte in the ice. To verify this, we sharply decrease the electric current to a value that is lower than the critical value for bundle formation when the bundles of the nanopearl chains have developed for a while. We observe that the morphology of electrodeposits changes back to the conventional fractal-like branches as we reported before [11] [Fig. 3(a)] and the detail morphology of the transition area is shown in Fig. 3(b).

Further, *in situ* optical interference contrast microscopy is applied to observe the growing interface during the bundle formation [Fig. 3(c)]. The uniform gray region far in front of the interface corresponds to the flat ice. Immediately adjacent, the growing tips there are separated regions with brighter contrast. Since the thickness of the deposition cell remains uniform in this process, the change of contrast therefore stands for the change of local refractive index. Figure 3 suggests that when the electric current in electrodeposition becomes sufficiently high, the generated heat cannot diffuse away in time. The accumulated heat melts the ice locally. When the melting rate is sufficiently high, the retreating interface of ice may become unstable and form cellular channels embedded in the ice. These channels eventually play the role of template to generate the parallel bundles.

To quantitatively analyze this growth behavior, we measured the average separation of the neighboring bundles, λ, when the electric current is changed between 20 to 40 μA. During each run of electrodeposition (with different applied electric current), the rest of the experimental conditions, such as the initial concentration of the electrolyte solution, the thermostat temperature, etc., are kept constant. The results are shown in Fig. 4 and the data can be fitted by $\lambda \propto I^{-0.525}$. The power index equals to −0.525, which will be compared to theoretical modeling later.

Figure 3 suggests that the formation of bundle pattern is related to the morphological instability of melting interface of ice. Now we try to relate the interbundle separation and the destabilized wavelength on the melting interface of ice. Following the method in Refs. [19,20], we apply linear stability analysis to the melting interface by superimposing a spatiotemporal disturbance $\delta(x,t)$ to the concentration field $C(x,t)$. Note that an arbitrary disturbance can always be expanded as a series of sine or cosine functions with different frequencies. Let the time-dependent amplitude of the disturbance be expressed as $\exp(\varpi t)$. Whether the concentration field is stable against disturbance is then determined by the sign of ϖ: a negative ϖ leads to a stabilized concentration field, whereas a positive ϖ results in an unstable concentration field. For the disturbance with positive ϖ, there exists a wave number q_m corresponding to the largest ϖ. The wavelength associated with q_m is then termed as the most dangerous destabilized wavelength λ_m [19], which is a function of the interfacial growth rate and hence a function of external control parameters in electrodeposition.

To model the interfacial instability, the coordinate system on the interface of electrodeposition is established as follows. The electrodeposits nucleate on the cathode and develop toward the anode. The growth direction of the deposits is defined as $+Z$ axis. The X axis is horizontally along the

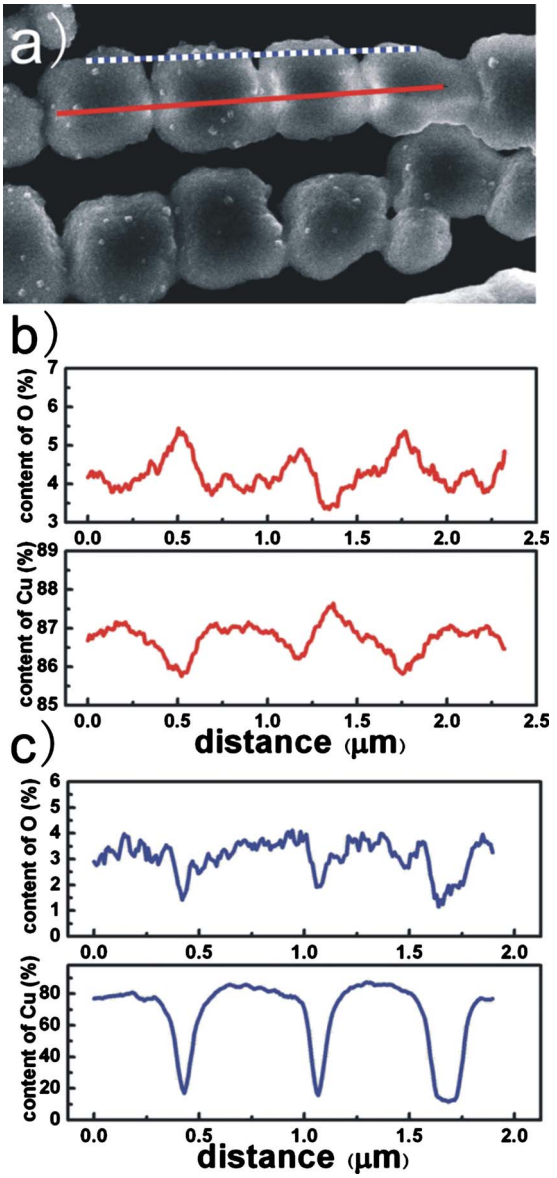

FIG. 2. (Color online) The EDS analysis of chemical components along different lines on the pearl-chain structure. The pearl chains were electrodeposited with electric current 30 μA. (b) shows the oxygen and copper distribution along the solid red (gray) line on the filament. It is clear that oxygen is more concentrated in between the beads, whereas on the bead the concentration of oxygen is lower. (c) shows measurements along the edge of the filament (along the dashed white line). The concentration of oxygen is much lower on the silicon surface than that on the copper bead.

growing interface of the electrodeposits, which is considered as infinitely long. The retreating of melting interface of ice is also along $+Z$. The interface moving velocity is defined as V and the driving force for ice melting, i.e., superheating, is defined as Δ. A schematic diagram of the growing interface is shown in Fig. 5.

Following Ref. [19], in the moving coordinate frame ($z'=z-Vt$), the diffusion equation ($\frac{\partial C}{\partial t}=D\nabla^2 C$) can be rewritten as $\frac{1}{D}\frac{\partial C}{\partial t}=\nabla^2 C+\frac{2}{l_D}\frac{\partial C}{\partial z'}$, where $l_D=\frac{2D}{V}$ is the width of the diffusion boundary layer. For the stabilized melting interface,

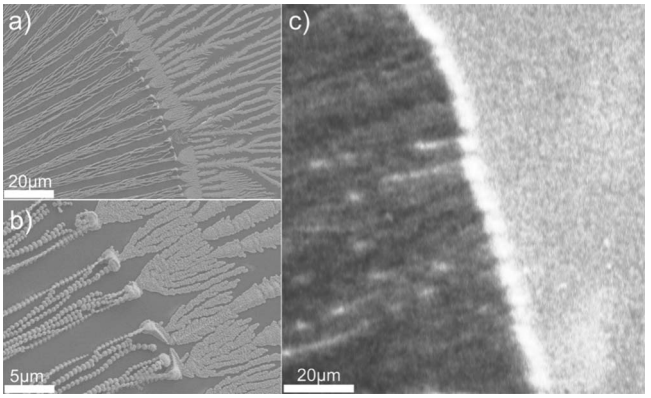

FIG. 3. [(a) and (b)] SEM micrographs to show the change of the deposit morphology when the electric current in electrodeposition of the filament bundles is suddenly decreased. (b) shows the enlarged micrograph of (a). Once the electric current is decreased, the deposit morphology changes from the bundles to the fractal-like filaments. (c) Optical interference contrast micrograph of the growing interface in electrodeposition. Bright spots can be identified in front of the growth front.

the diffusion field does not vary with time in the moving coordinate frame, i.e., $\frac{\partial C}{\partial t}=0$. This leads to $\nabla^2 C+\frac{2}{l_D}\frac{\partial C}{\partial z'}=0$. For one-dimensional concentration field, the equation can be simplified as $\frac{d^2C}{dz'^2}+\frac{2}{l_D}\frac{\partial C}{\partial z'}=0$ and the solution is in the form of $C(z')=A\exp(-\frac{2}{l_D}z')$ or $C(z,t)=A\exp[-\frac{2}{l_D}(z-Vt)]$. The coefficient A can be determined from the boundary conditions. Now we introduce a spatiotemporal disturbance $\delta(z,t)$ to this one-dimensional concentration field $C(z,t)$. An arbitrary random disturbance can be expanded as a series of sine or cosine functions with different frequencies. Here we concentrate on the behavior of a disturbance component with wavelength λ and investigate the response of the growth interface to this disturbing component. The disturbed interface can be expressed as

$$z(x,t)=Vt+\delta\exp(\varpi_q t)\cos\left(\frac{2\pi}{\lambda}x\right), \tag{1}$$

where the sign of ϖ_q determines the stability of the interface, as we mentioned before. Since the shape of the interface also influence the diffusion field $C(z,t)$, the disturbed concentra-

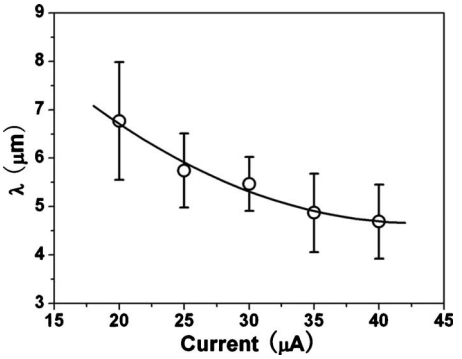

FIG. 4. The interbundle separation measured on the samples that electrodeposited with different electric current.

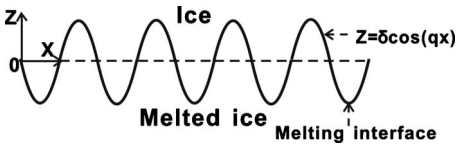

FIG. 5. The schematics of the disturbed melting interface of electrolyte ice in our system.

tion field can be taken as a superposition of the concentration field of a flat interface together with a term originates from interface deformation. The latter term should vanish far away from the interface. With all these considerations, the concentration field in front of the disturbed interface is expressed as

$$C(x,z,t) = A\ \exp\left[-\frac{2(z-Vt)}{l_D}\right] + \delta C_q\ \exp(\varpi_q t) \times\cos\left(\frac{2\pi}{\lambda}x\right)\exp[-\Lambda_q(z-Vt)], \tag{2}$$

where Λ_q is the damping coefficient of the concentration field and the subscript q defines the component associated with the disturbance wave number $q=\frac{2\pi}{\lambda}$.

By taking the disturbed concentration field into diffusion equation $\frac{\partial C}{\partial t}=D\nabla^2 C$, we obtain the relation

$$\frac{\varpi_q}{D}+2\frac{\Lambda_q}{l_D}=-q^2+\Lambda_q^2. \tag{3}$$

In addition, local equilibrium condition on the interface requires $C_i=\Delta-d\kappa$, where C_i is the local concentration at the interface, Δ is the superheating, d is the capillary length, and $\kappa\approx-\frac{\partial^2 z}{\partial x^2}$ is the curvature [19]. By neglecting the higher-order infinitesimal terms, it follows that

$$\delta C_q=\left(\frac{2}{l_D}\Delta-dq^2\right)\delta. \tag{4}$$

On the other hand, continuity condition at the interface requires $V_z=-D\frac{\partial C}{\partial z}$, which can be written as $-\frac{1}{D}\frac{\partial z}{\partial t}=\frac{\partial C}{\partial z}$. By taking Eqs. (1) and (2) into this expression and neglecting higher-order terms, we get $A=\Delta=1$ and

$$\frac{\varpi_q}{D}=\frac{\Lambda_q\delta C_q}{\delta}-\left(\frac{2}{l_D}\right)^2. \tag{5}$$

Combining Eqs. (4) and (5), we get

$$\frac{\varpi_q}{D}=-\left(\frac{2}{l_D}\right)^2+\left(\frac{2}{l_D}-dq^2\right)\Lambda_q. \tag{6}$$

From Eqs. (3) and (6), we can determine the damping coefficient Λ_q as $\Lambda_q=\frac{2}{l_D}-\frac{1}{2}dq^2+|q|\sqrt{1-\frac{2d}{l_D}+\frac{d^2q^2}{4}}$ and the dynamic coefficient of the disturbance can be expressed as

$$\frac{\varpi_q}{D}=\left(\frac{2}{l_D}-dq^2\right)|q|\sqrt{1-\frac{2d}{l_D}+\frac{d^2q^2}{4}}-\frac{3dq^2}{l_D}+\frac{d^2q^4}{2}. \tag{7}$$

In our experiments, the growth velocity $V\sim 1.0\ \mu$m/s and the diffusion constant $D\sim 10^{-6}$ cm^2/s, consequently

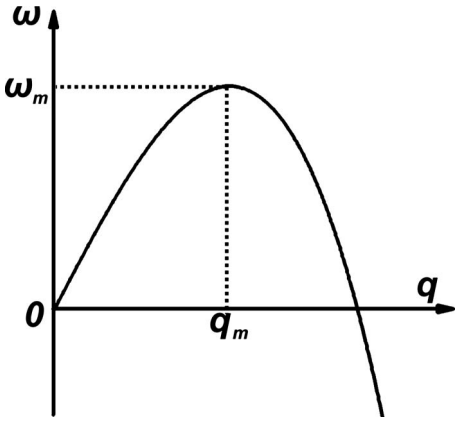

FIG. 6. The schematics to show the dispersion relation as that shown in Eq. (8).

$l_D\sim 100\ \mu$m. The capillary length is defined as $d=\frac{\gamma}{L}\frac{T_M}{L/C_P}$, where L, γ, T_M, and C_p represent the latent heat per volume, the surface free energy, the melting temperature, and the specific heat per volume, respectively [19,20]. The capillary length is of the order of $10^{-3}\ \mu$m. The disturbed wavelength λ is roughly of the order of $1-10\ \mu$m. Hence, we have $d\ll\lambda<l_D$. Therefore, Eq. (7) can be simplified as

$$\frac{\varpi_q}{D}=\left(\frac{2}{l_D}-dq^2\right)|q|. \tag{8}$$

The plot of $\varpi_q(q)$ described by Eq. (8) is schematically shown in Fig. 6. It is noteworthy that there exists a wave number q_m that leads to the maximum dynamic response (largest ϖ_m), which can be determined from $\frac{\partial\varpi_q}{\partial q}=0$. The wavelength corresponding to q_m is defined as the unstable wavelength λ_m. It follows that λ_m can be expressed as

$$\lambda_m=2\pi\sqrt{\frac{3dD}{V}}. \tag{9}$$

According to the electrochemical growth theory developed by Chazaviel [21], the interfacial growth rate is proportional to the electric current in electrodeposition. Therefore, Eq. (9) can be rewritten as

$$\lambda_m\propto\frac{1}{\sqrt{I}}=I^{-0.5}. \tag{10}$$

We expect that this wavelength corresponds to the spatial separation of the neighboring molten channels in electrolyte ice. Note that the power index in Eq. (10) is −0.5, which is very close to the experimental value −0.52. We therefore conclude that the bundle separation of the electrodeposits is associated with λ_m and theoretical modeling is consistent with experimental observations.

In template-assisted growth, specially designed template is applied to regulate the growth by controlling the local nucleation energy barrier and the nucleation rate. For the scenario of this paper, however, the template is not defined in advance. Instead, it is decided by the instability during the melting of electrolyte ice, which is attributed to the heat generation in electrodeposition. So this is a self-perpetuating

process. The periodically melted channels change the nucleation and growth environment (locally enhanced mass transport), eventually generate the periodically distributed bundles of copper filaments. This self-templating growth behavior, to the best of our knowledge, has not been reported before and could be used to generate ordered metallic patterns with hierarchical structures.

As demonstrated in Fig. 2, and also in previous papers [10,11], the periodic structures on each individual filament actually correspond to the alternating deposition of copper and cuprous oxide. Despite of periodic distributions of Cu and Cu_2O along the filament, a conductive core should exist inside of each filament, since the filaments are electrodeposited. The spatial periodicity along the filament can be tuned by changing the applied electric current in electrodeposition. Here in this experiment, the window to observe the bundle formation is narrow (about 30 μA), so we did not observe the evident change of spatial periodicity along each individual filament when the electric current is changed. Since the formation of the corrugated periodic structures results from the competition of mass transfer and interfacial kinetics in electrodeposition, we therefore expect that the periodicity along the filament may also be modified by changing temperature and concentration of the electrolyte as well.

To summarize, we provide here an approach to fabricate arrays of nanostructured metallic filaments with tunable bundle separation, which is induced by instability of melting electrolyte ice during electrochemical deposition in the ultrathin layer when the Joule heat cannot be released in time. The bundle separation can be tuned by changing the applied electric current. The equally separated bundles consist of long, straight, pearl-chain-like copper filaments with corrugated periodic structure. This unique electrochemical deposition behavior provides an interesting example to understand pattern formation and demonstrates an interesting approach to fabricate ordered structures by self-organization.

ACKNOWLEDGMENTS

This work has been supported by the Ministry of Science and Technology of China (Grants No. 2004CB619005 and No. 2006CB921804), by the National Natural Science Foundation of China (Grants No. 10625417 and No. 10874068), and by Jiangsu Province (Grant No. BK2008012).

[1] D. Appell, Nature (London) **419**, 553 (2002).
[2] K. S. Shankar and A. K. Raychaudhuri, Mater. Sci. Eng., C **25**, 738 (2005).
[3] Z. L. Wang, *Nanowires and Nanobelts—Materials, Properties and Devices* (Kluwer Academic Publishers, Boston, 2003).
[4] Y. Xia, P. Yang, Y. Sun, Y. Wu, B. Mayers, B. Gates, Y. Yin, F. Kim, and H. Yan, Adv. Mater. **15**, 353 (2003).
[5] V. Fleury, W. A. Watters, L. Allam, and T. Devers, Nature (London) **416**, 716 (2002).
[6] V. Fleury and D. Barkey, Physica A **233**, 730 (1996).
[7] V. Fleury, Nature (London) **390**, 145 (1997).
[8] M. Rosso, E. Chassaing, and J. N. Chazalviel, Phys. Rev. E **59**, 3135 (1999).
[9] M. Rosso, E. Chassaing, J. N. Chazalviel, and T. Gobron, Electrochim. Acta **47**, 1267 (2002).
[10] M. Wang, S. Zhong, X. B. Yin, J. M. Zhu, R. W. Peng, Y. Wang, K. Q. Zhang, and N. B. Ming, Phys. Rev. Lett. **86**, 3827 (2001).
[11] S. Zhong, Y. Wang, M. Wang, M. Z. Zhang, X. B. Yin, R. W. Peng, and N. B. Ming, Phys. Rev. E **67**, 061601 (2003).
[12] B. Zhang, Y.-Y. Weng, X.-P. Huang, M. Wang, R.-W. Peng, N.-B. Ming, B. Yang, N. Lu, and L.-F. Chi, Adv. Mater. **21**, 3576 (2009).
[13] C. Genet and T. W. Ebbesen, Nature (London) **445**, 39 (2007).
[14] P. Lalanne and J. P. Hugonin, Nat. Phys. **2**, 551 (2006).
[15] Y.-J. Bao, R.-W. Peng, D. J. Shu, M. Wang, X. Lu, J. Shao, W. Lu, and N.-B. Ming, Phys. Rev. Lett. **101**, 087401 (2008).
[16] S. A. Maier, S. R. Andrews, L. Martin-Moreno, and F. J. Garcia-Vidal, Phys. Rev. Lett. **97**, 176805 (2006).
[17] Z. Wu, H. M. Li, X. Xiong, G. B. Ma, M. Wang, R. W. Peng, and N.-B. Ming, Appl. Phys. Lett. **94**, 041120 (2009).
[18] J. A. Switzer, C. J. Hung, L. Y. Huang, E. R. Switzer, D. R. Kammler, T. D. Golden, and E. W. Bohannan, J. Am. Chem. Soc. **120**, 3530 (1998).
[19] Y. Saito, *Statistical Physics of Crystal Growth*, 1st ed. (World Scientific Publishing Company, Singapore, 1996).
[20] N.-B. Ming, *Fundamentals of Crystal Growth Physics* (Shanghai Science and Technology Press, Shanghai, 1982).
[21] J.-N. Chazalviel, Phys. Rev. A **42**, 7355 (1990).